CCFE
CULHAM CENTRE FOR FUSION ENERGY

UK Atomic Energy Authority

UKAEA-CCFE-CP(23)18

J. Morris, M. Coleman, S. Kahn, A. J. Pearce, D. Short, J. E. Cook, S. Desai, L. Humprey, M. Kovari, J. Maddock, D. Vaccaro

Preparing systems codes for power plant design

Preparing systems codes for power plant design

J. Morris, M. Coleman, S. Kahn, A. J. Pearce, D. Short, J. E. Cook,
S. Desai, L. Humprey, M. Kovari, J. Maddock, D. Vaccaro

This paper has been submitted to
28th IAEA Fusion Energy Conference, Nice, France, 10-15th May 2021

PREPARING SYSTEMS CODES FOR POWER PLANT CONCEPTUAL DESIGN

J. Morris*, M. Coleman, S. Kahn, S. Muldrew, A. J. Pearce, D. Short,
J. E. Cook, S. Desai, L. Humphrey, M. Kovari, J. Maddock, D. Vaccaro
United Kingdom Atomic Energy Authority
*Email: james.morris2@ukaea.uk

Abstract

As power plant design programmes approach the transition between the pre-conceptual and conceptual design phases the systems code PROCESS has been improved to incorporate more detailed plasma physics, engineering, and analysis modules. Unlike many systems codes, PROCESS combines the physics modelling with both technology and costs analysis. Some of the key topics in the conceptual design phase are toroidal field magnet design, divertor power handling, operational sensitivity, and economic uncertainty analysis. Models covering these areas have been integrated or improved in PROCESS. During pre-conceptual design, systems codes are an essential tool for exploring fusion power plant concepts. They allow one to model the interaction of the plant systems and quickly perform reactor optioneering. To be able to carry out these large scoping studies, the fidelity of the models can be restricted to reduce the computational time. For example, the EUROfusion EU-DEMO baseline designs are created using the systems code PROCESS and the ability to measure these trade-offs has led to important design choices being examined during the DEMO pre-conceptual design phase. Ruling out unfeasible designs allows one to efficiently identify where in the design space to carry out detailed design work. The paper describes how PROCESS has begun retooling for use in later stages of power plant conceptual design. Details are given for new additions to the PROCESS uncertainty quantification tools, high-temperature superconducting magnet model, toroidal field coil model, and new models for spherical tokamaks (STEP). Additionally, the paper covers recent developments on the novel systems code BLUEPRINT which is being used in both the EUROfusion and STEP projects. The paper concludes with an outlook on systems code activities at UKAEA and work with external partners.

1. INTRODUCTION

In nuclear fusion research, systems codes are used to rapidly analyse large parameter spaces to find optimised power plant design solutions that are self-consistent. The models in systems codes are typically 0-D and 1-D simplified calculations with the aim of capturing the key physics and engineering processes while being computationally inexpensive. During the pre-conceptual design phase of a fusion reactor, systems codes can provide useful insight into the trade-offs between machine systems, which are often not intuitive, and can provide an optimised design as a starting point for more detailed analysis. Systems codes can also take advantage of their speed by allowing users to investigate large groups of design points to understand the parameter space and perform uncertainty analysis. As the power plant design programmes approach the transition between the pre-conceptual and conceptual design phases the use case for systems codes requires that they offer more detailed insight into the plant systems. The systems code PROCESS [1], [2] has been in activate development at UKAEA for over 20 years and has been used heavily in the EUROfusion DEMO programme [3]–[6] as well as other reactor projects such as CFETR [7] and STEP [8]. The systems code PROCESS has been improved to incorporate more detailed plasma physics, engineering, and integration models. Unlike many systems codes, PROCESS combines the physics modelling with both technology and costs analysis. The paper will outline the areas targeted for improvement and expand on their use so far. With a view to delivering higher fidelity reactor designs, UKAEA has also been developing a reactor design framework, BLUEPRINT [9], in which several models and codes (including PROCESS) are used in conjunction to automate fusion reactor design. The BLUEPRINT code starts from a PROCESS output and carries out more detailed analysis, such as: free-boundary equilibrium solutions, generation of 3-D CAD output, tritium fuel cycle, and more. In the paper, the power plant conceptual design phase workflow is outlined as well as the key system code requirements in Section 2, the enhancement of the systems code PROCESS is detailed in Section 3, progress on the BLUEPRINT reactor design framework is described in Section 4, and Section 5 provides a summary and outlook.

2. CONCEPTUAL DESIGN PHASE AND SYSTEM CODE REQUIREMENTS

In a fusion power plant design cycle, systems codes form the first step in the analysis workflow. For example, Figure 2 from [9] shows the EU-DEMO design workflow and where systems codes like PROCESS fit into the design cycle. Typically, in a power plant pre-conceptual design phase systems codes have been used to carry out:

— Parameter space investigations – aspect ratio scans, major radius scans, investigation of divertor protection parameters [10], and alternative machine configurations such as "Flexi-DEMO" [11].
— Uncertainty quantification [4], [7] – applying distribution functions (e.g. uniform, Gaussian, half-Gaussian) to PROCESS input parameters and analysing the impact to machine design.
— Cost analysis – updating unit costs measurements with up-to-date costing data where available. Providing important relative costing information as well as estimating cost of electricity and upfront capital cost. PROCESS is being used for costing analysis on the STEP project.
— Collaborations with other fusion research programmes to analyse reactor concepts such as SST-2 [12], stellarator power plants [13], [14], and CFETR [7].

As power plant design programmes move into the conceptual design phase, the use cases for systems codes expands into other areas of interest. Going forward there will be a need to have the additional capability to perform:

— More detailed costing analysis of a given concept design. Providing estimates with uncertainties on the sub-system costs, up-front capital cost, and the cost of electricity.
— Uncertainty quantification on power plant designs that have fixed geometry and engineering parameters, determining the impact of underperformance and solutions to recover performance.
— More detailed models for plant sub-systems, expanding coverage of 1-D and 2-D models.
— Generate 3-D CAD of the machine design rapidly for use with detailed codes (e.g. neutronics).

3. ENHANCEMENT OF SYSTEMS CODE PROCESS

The ability to measure plant system trade-offs has led to important design choices being examined during the DEMO and STEP pre-conceptual design phases. Ruling out unfeasible design points allows the plant integration team to efficiently identify where in the design space to carry out detailed design work. The paper describes how PROCESS has been retooled for more detailed power plant concept design.

3.1. Uncertainty tools

Sensitivity analysis can be used to identify the most consequential parameters of a given model and is a powerful method of analysing complex models. In systems codes for fusion power plant design, these analysis methods can be used to establish what the main drivers of design outcomes are and allows for the identification of areas of additional technical focus and uncertainty propagation. Within PROCESS a new sensitivity analysis method has been implemented, here we will outline the technique and give an example use case.

The method of elementary effects, which is also known as the Morris method, is a sensitivity measure for ranking the parameters in order of effect on a model output [15]. This method is relatively computational inexpensive as compared to variance-based methods and allows for the identification of negligible variables and for the screening of the most important parameters for more intensive study. We consider the PROCESS model as $y(\boldsymbol{X})$ where $\boldsymbol{X} = (X_1, X_2, \ldots, X_k)$ is the i-th model input of set of k inputs considered. We can sample the input space in a k-dimensional hyper cube discretised into p levels. Each elementary effect is computed by considering a set of trajectories through the input space, which is sampled from randomly selected initial points. For a given input X, the elementary effect of the i-th input factor is defined by

$$EE_i^j = \frac{y(\boldsymbol{X}+\boldsymbol{e}_i\Delta) - y(\boldsymbol{X})}{\Delta}.$$

Where here $\boldsymbol{e}_i$ is the orthonormal basis vector for the i-th dimension of the input space hyper cube and the level spacing Δ is given by $\Delta = p/(2(p-1))$. For more information on this sensitivity measure see [16]. Once we have computed the elementary effects, we study their distribution to identify sensitivity measures using the two expressions,

$$\mu_i^* = \frac{1}{r}\sum_{j=1}^{r}\left|EE_i^j\right| \qquad \sigma_i^2 = \frac{1}{r-1}\sum_{j=1}^{r}\left(EE_i^j - \mu_i\right)^2$$

where μ_i^* is the absolute mean of the elementary effects of the i-th parameter and σ_i is the standard deviation of the elementary effects of the i-th model parameter. The absolute mean gives a ranking of the effect of an input on model output allowing for the identification of negligible model inputs. While the standard deviation gives an estimation of the linearity of the model input, where $\sigma_i = 0$ indicates a linear parameter which does not interact with other model inputs in determining the model output.

In Figure 1 we present a scatter plot of the absolute mean and standard deviation of the elementary effects for each parameter for the figure of merit of maximising fusion gain Q while considering its effect on machine capital cost. Comparing between optimising for a minimal major radius and machine capital cost we see broad agreement in the ranking of the effects on the capital cost. The one extreme outliner in determining the capital cost is P_{LH} the LH threshold, which in turn is followed by the lower bound plasma safety factor and the maximum peak toroidal field. When optimising a DEMO-like machine for the maximum fusion gain, PROCESS consistently finds solutions in the high magnetic field and high plasma current regime with $B_T(R_0) > 6\ T$ and $I_p > 22\ MA$, and where P_{sep} is minimal for H-mode operation, satisfying $P_{LH} = P_{sep}$. Because of the fixed radial build, this sets strong constraints on the parameter space explored as the Martin scaling for the LH-threshold reduces to a function of on-axis toroidal field and density $P_{LH} \sim n_{20}^{0.717} B_T^{0.803}$. In this scenario the design of magnets which influences the magnetic energy in the plasma, is the largest underling driver of cost.

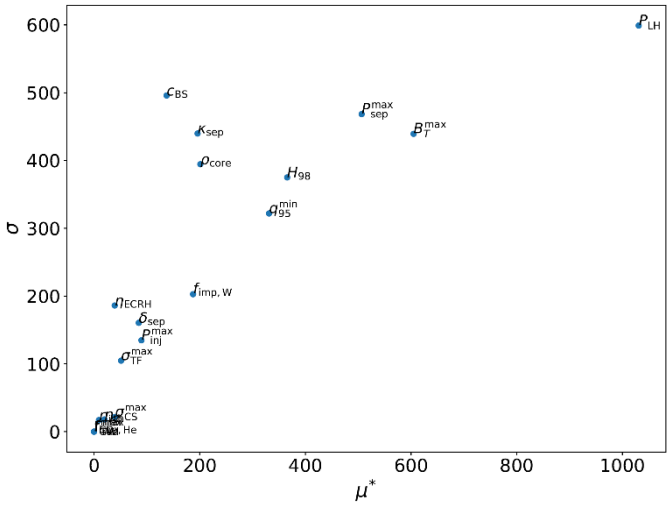

Figure 1: plot of the absolute mean against the standard deviation of the elementary effects for each parameter for a 9m DEMO-like machine with a fixed radial build, requiring Pnet,el ≥ 400MW and using the fusion gain Q as the figure of merit.

3.2. Advanced divertor designs

In a reactor-relevant machine, the heat exhaust problem has been identified as amongst the most crucial challenges to be overcome. A proposed solution to this problem is the use of advanced divertors designs, which are divertor solutions which utilise complex magnetic configurations to increase wetted area, divertor volume, and closure. The novel scrape-off-layer physics regimes exploited by these designs also comes with additional engineering constraints and challenges, therefore the trade-offs of these solutions must be investigated. The divertor geometry calculation has been updated within PROCESS. This has been done to increase the model's flexibility and able to capture divertor geometry allowing for an investigation of advanced designs. The more detailed control over the divertor structure allows for the long legged divertor used in advanced designs and the PROCESS optimisation routines and other physics and engineering modules will allow for the study of how advanced divertors may affect other reactor subsystems. Here we will discuss the X-divertor [17] and Super X-divertor [18]. In previous studies we have looked at double-null divertor configurations using PROCESS [19], and we leave the proposed snowflake divertor for future study.

For these studies we will use the Kallenbach model, which is a 1-D scrape-off-layer model for the outer divertor that has been implemented in PROCESS based on the model presented in [20]. This model is derived using some assumptions which could prove invalid, in the highly radiative and large flux expansion regime of advanced divertors, but we will use this model as the beginning of this investigation. Firstly, the model assumes operation in the partially detached regime, and secondly in a scrape-off-layer with high flux expansion we expect increased importance of cross field transport, which cannot be captured in a one-dimensional model. The existing calculation is independent of the poloidal length of the outer leg $L_{p,o}$, to understand the role of the long legged divertor like the SX-divertor, and to understand how the Kallenbach model treats impurity radiation in the long-legged regime, we perform scans of two cases, one with $L_{p,o} = 1.0m$ and one with $L_{p.o} = 3.0m$ and

both optimising for a minimised major radius. Increasing $L_{p,o}$ increases the radius of the strike point which increases the pitch angle and flux expansion due to the decrease in the toroidal field at the target. In Figure 2 we present the outcome of these scans in connection length of the radiated power in the scrape-off-layer P_{rad}, and the fraction of the power enter the scrape-off-layer at the outer mid plane which is radiated f_{rad}.

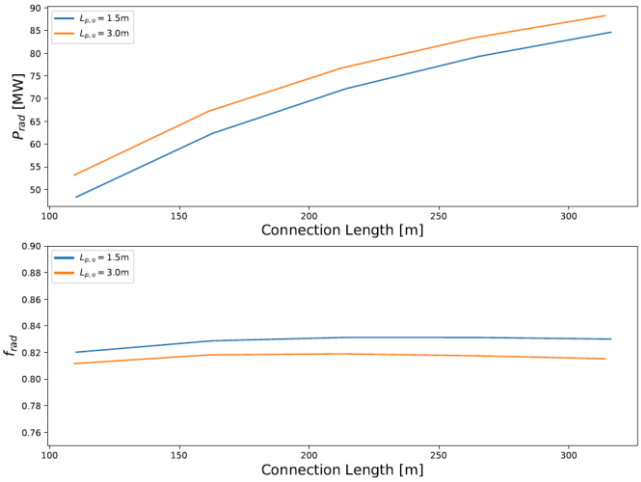

Figure 2: The total P_rad and fraction f_rad of power radiated in the scape-off-layer solutions under a scan of the connection length. All scans done with the Kallenbach model using λ_{omp} = 2mm, λ_t = 9mm giving f_x = *3.39*.

We observe in these plots that volumetric power loss is approximately constant but the due the rise in the connection length there are much higher integrated radiation power losses. We also note that all increase in flux expansion arises from changing magnetic field at the target as we keep $\lambda_t = 9mm$ in both cases, and the increase in flux expansion raises the $P_{rad,sol}$~5 MW. This highlights the need to a more accurate model of the magnetic field at the divertor target as it can cause changes of up to 10% in the radiated power in the scape-off-layer. This issue can be solved with future work using a free boundary equilibrium solver, which would provide a good value for the field strength at the target.

3.3. High Temperature Superconductor - REBCO

One of the primary drivers of machine design, performance and cost are the superconducting magnets. Therefore, correctly calculating the space required, the achievable field, and cost is essential for PROCESS. High temperature superconductors (HTS) can potentially offer a performance, engineering, and cost benefits. A REBCO (rare earth barium copper oxide [21]) HTS model has been written for PROCESS for the TF coils. The operating temperature of the TF coil for both LTS and HTS is 4.5 K for the analysis presented here as it is often preferable to go to higher field to achieve large net electric power, as the fusion power is proportional to β^2B^4. PROCESS has been used to analyse the impact of toroidal field coil stress on machine design with LTS [3] and can now compare with HTS. Figure 3 shows the effect of the allowable Tresca stress in the TF coil steel. The LTS model includes a quench calculation with a variable copper fraction, while the HTS model imposes a maximum superconductor current per unit area of copper, chosen as 100 A/mm^2 or 200 A/mm^2. PROCESS was set to minimise the major radius and to produce 500 MW net electric power for 2 hours. Figure 1 shows that one can achieve higher fields at smaller machine size with HTS. The reduction in major radius depends on the copper requirement and is in the range 0.25-0.5m. At higher allowable stress, the HTS PROCESS runs start to prioritise smaller machine size over further increasing the field.

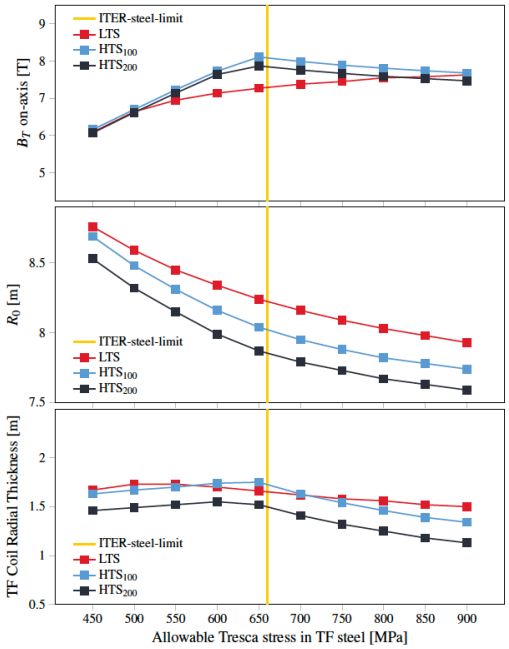

Figure 3: Results of PROCESS runs in which the allowed Tresca Stress in the TF coil structural material is increased while minimising the major radius. “LTS” represents Nb3Sn using the WST parameterisation. “HTS” represents REBCO tape for 100 and 200 A/m

3.4. Spherical Tokamaks in PROCESS

Spherical tokamaks offer several physics advantages that make them an attractive option for future fusion power plants (See [22] for a recent review). Typically defined by an aspect ratio of less than 2, spherical tokamaks operate at significantly higher beta (ratio of plasma pressure to magnetic pressure) and generate larger bootstrap currents compared with conventional aspect ratio machines. The high contribution from the bootstrap current can eliminate the need for inductive current, removing the requirement for a central solenoid and allowing steady-state operation. A combination of these benefits leads to smaller, and potentially cheaper, power plants. The converse challenge is to the engineering, where neutron and heat loads will be higher due to the compact configuration.

Within PROCESS there are a number of spherical tokamak specific options that can be applied, and these were last outlined in [8]. PROCESS is under continuous development meaning further updates have been applied since then. The main difference in the engineering between the conventional and spherical tokamaks is in the toroidal field (TF) coils. High beta plasmas allow for low field devices, and this has previously led to spherical tokamak power plants being proposed with resistive TF coils, e.g. ARIES-ST [23] and STPP [24]. PROCESS has the option of using a resistive monolithic centre-column, with either picture frame or D-shaped return limbs. One of the biggest impacts of resistive coils on the overall plant design is the resistive losses that must be compensated for. To minimise resistive losses, the centre-column is tapered, being thinnest at the midplane where space is tightest and widening at the top. This hourglass shape reduces the resistance of the centre-column and hence reduces the power losses. Several alternative options for the plasma physics have been added for spherical tokamaks. Many of the original plasma scaling in PROCESS come from the ITER Physics Design Guidelines: 1989 [25] and were formulated for conventional aspect ratio devices. [8] fitted a set of spherical equilibria generated with FIESTA, a free-boundary equilibrium code, to generate a new plasma current relation:

$$I_p = 2.69\left(\frac{a^2 B_t}{R_0 q_{95}}\right)(1.0 + 2.44\epsilon^{2.736})\kappa_x^{2.154}\delta_x^{0.06}$$

Where R_0 is the major radius, a the minor radius, ϵ is the inverse aspect ratio (a/R_0), κ_x is the x-point elongation and δ_x is the x-point triangularity. Subsequently, we have updated the relations between x-point and 95% values, as these are not the same for spherical tokamaks as given in the ITER design guidelines. Further fitting to FIESTA gave:

$$\kappa_x = 0.91\kappa_{95} + 0.39$$

We compared this to a selection of MAST shots and found good agreement. For the triangularity, a clear relation was not easy to develop due a dependence on the Poloidal Field (PF) coil layout. From fitting to FIESTA and MAST we found:

$$\delta_x = 1.38\delta_{95} + 0.05 \quad \text{(FIESTA)} \qquad \delta_x = 0.77\delta_{95} + 0.19 \quad \text{(MAST)}$$

Both equations are included in PROCESS as options that can be used. The composition of the plasma current is very important to the overall design point, especially as, without inductive current, all non-self-driven current needs to come from the heating and current drive system. We typically use the Sauter, Angioni & Lin-Liu (1999) model [26] to calculate the bootstrap current, however other models are available within PROCESS. These models are the same models used for conventional aspect ratio. We have added relations for the diamagnetic current and Pfirsch-Schlüter current, additional self-driven currents, based on fitting to equilibria generated with the fixed-boundary equilibrium code SCENE [27]:

$$\frac{I_{dia}}{I_p} = 0.414\,\beta\left(0.1\,{}^{q_{95}}/_{q_0} + 0.44\right) \qquad \frac{I_{PS}}{I_p} = -0.09\,\beta$$

The energy confinement time scaling for spherical tokamaks is highly uncertain due to the limited data available. We have added the NSTX and NSTX-Petty hybrid scalings [28], however typically use the IPB98(y,2) scaling [29]. We enforce the beta limit at the higher spherical tokamak value of β_N<6 [30].

3.5. Toroidal field coil magnet model

3.5.1. Inboard mid-plane stress model

The inboard mid-plane section is a crucial sector for most TF coil design. As structural support can represent a non-negligible fraction of inboard space [6], its associated material stress must be calculated with care during the design optimisation. In the previous PROCESS stress model, mid-plane stresses was decoupling from the vertical one, adding it *a posteriori* as a constant [2], [3]. This method is only valid if the vertical dimensions are small and therefore should not be used for the stress calculation. Instead, the generalized plane strain (constant vertical normal strain) assumption should be used. The PROCESS stress model has been derived from first principle using this formulation. The model accounts for the current-carrying winding pack (WP) having different properties in the vertical and the mid-plane direction. Finally, the model has been extended to support any number of cylindrical layers, paving the way to integrate a wider variety of TF coil structural designs (e.g. graded coils).

The first structural design considered is the CS-TF bucking configuration. This allows a reduction of the TF coil support structure but increases the TF-CS interface complexity as the CS and the TF coils vary in vertical size in opposite direction when energized. A sliding interface must therefore be used to avoid friction, decoupling the TF coil vertical tension from the CS. The effect of this design on the inboard mid-plane TF coil stress has been implemented in PROCESS by adding another inward cylindrical layer representing the CS coil system. No electromechanical body forces have been considered in the CS layer as the most demanding configuration is when no current is flowing in the CS coil. As a sliding interface is needed, no vertical strain coupling is considered in the model between the TF and the CS coil systems. It is also important to note that such design will introduce some load variation causing fatigue on the TF coils and modifying the CS fatigue; this aspect is not currently captured. The model has been used to assess the benefits of a CS-TF bucking on a DEMO-like design. Figure 4 shows the radial displacement, normal strain and steel structure stress output from the PROCESS stress model. Three regions are visible: the CS coil region on the left of each plots, the support structure (case nose) in the middle and the winding pack on the right of each plots. The vertical strain is constant in the CS and the TF regions, in agreement with the plane strain assumption. The relatively high vertical strain in the CS layer is understood to be due to Poisson's ratio effects and the relatively weak CS structural properties on the vertical direction. We can also observe that no CS vertical stress is present as the CS coil. The middle segment, corresponding to the individual TF coil support structure, appears to be much thinner than winding pack, the CS coil being the support of the coil. Table 1 shows the comparison between a DEMO-like design with and without the CS-TF bucking. Although sizable TF coil inboard thickness reduction (due to a strong reduction of the support structures) has been achieved only a small major radius reduction is obtained, a hint that power plant design is not driven by TF coil constraints, but rather by exhaust and other constraints [10].

	R_0 [m]	B_T [T]	Aspect ratio	ΔR_{TF} [m]
Wedged TF	8.79	4.84	2.84	1.219
CS-TF bucking	8.58	4.54	2.67	0.962

Table 1: comparison between a DEMO-like design, minimising plasma major radius with and without the CS-TF bucking

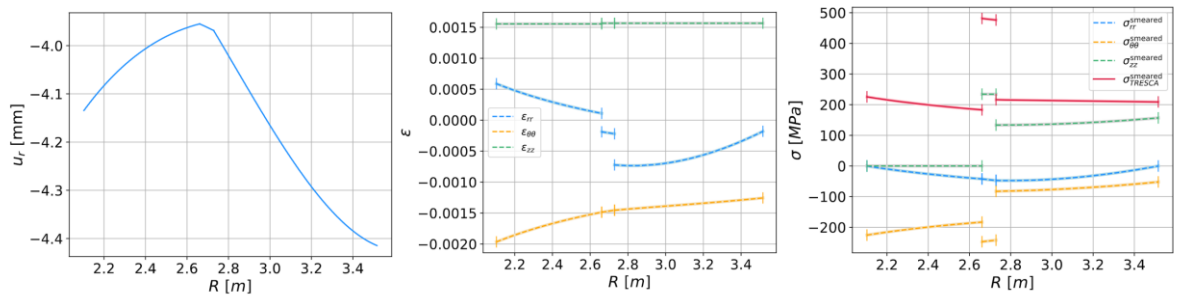

Figure 4: PROCESS stress analysis output for a CS-TF bucking structural design based on the DEMO-like design. The left plot shows the radial displacement as a function of the radial position. The middle plot shows the normal strain in the radial (blue) hoop (yellow) and the vertical (green) direction. And the right plot shows the steel structure normal stress radial distribution in the radial (dashed blue), hoop (dashed yellow), vertical (dashed green), and TRESCA stress criteria (red), used to assess the structural stress limits.

A second application under development will be the TF coil winding pack grading. Modifying the turn design with the turn radial position can be beneficial as its magnetic field decreases moving from the plasma side to the machine centre side, allowing using gradually less superconductor moving toward machine centre. On the other hand, the need for hoop stress support structure gradually increases going radially inward. Adapting the turn design will reduce the WP thickness with reduced support structure on the plasma side and reduced conductor space toward the machine centre, reaching lower aspect ratios and reducing cos. The structural effect of this design is already available in PROCESS as the turn-layer structural properties can be modified and optimized. However, the effect of varying magnetic field strength is not integrated for now as detailed on coil ripple must be considered first. This should be done in the future using a metamodel based on ripple calculations made with either the FIESTA code or the BLUEPRINT ripple calculations.

3.5.2. Vertical tension

The inboard mid-plane vertical tension previously was calculated under the assumption of an infinitely thin Princeton-D shape coil without any sliding joints. However, the WP finite thickness tends to reduce the total vertical force compared to the infinitely thin case. The analytical vertical tension calculation has been updated consider this effect. Another implicit assumption of the previous calculation is that the vertical tension splits equally between the inboard and the outboard TF coil leg. This is only true for a Princeton-D shape, for example, more vertical tension will be transferred to the inboard leg if rectangular coils are used. An analytical formula providing the vertical tension split has been developed for picture frame coils but has not yet been implemented in the code. The presence of sliding joints also modifies the vertical tension split. This effect is now calculated in PROCESS using an analytical derivation.

3.5.3. Development for spherical tokamaks (ST)

Neglecting the out-of-plane loads, the TF coil outboard leg electromechanical forces are relatively small on a spherical tokamak as both the plasma major radius and toroidal field are relatively small for spherical tokamaks. This allows the use of a picture frame coil to provide space for long-legged divertor configurations and easier remote maintenance. Therefore, rectangular TF coil shapes has been added in PROCESS. Similarly, tapered geometry can be used for resistive coils to minimize resistive heating keeping low aspect ratio. Finally, sliding joints, that decouple the TF coil vertical strain from the inboard and outboard sides of the TF coil can be used in PROCESS. Its design is assumed to be the same as that of MAST [35] and ALCATOR C-mod [36], and its resistive heating is estimated using joints measurement from ALCATOR C-Mod [36]. Its structural impact on inboard TF coil stress is estimated by calculating the vertical tension split as mentioned in the Section 3.5.2.

3.6. PROCESS Structural changes

The PROCESS systems code was originally written entirely in FORTRAN, which has several drawbacks when compared with modern scientific computing paradigms. These revolve around its impenetrability, resulting in a steep learning curve for new collaborators, difficulties in testing and debugging and difficulties integrating with other tools or codes. To solve these problems, the FORTRAN executable has been converted to a library which can be imported by a Python package; this maintains the existing FORTRAN models and solver but provides the easy access and object-orientated benefits of Python. The Python package imports an interface layer which exposes the necessary FORTRAN to allow the rest of the FORTRAN library (solver, models) to run based on values passed from the Python layer. The PROCESS Python package is object-orientated and allows for easier debugging in modern Integrated Development Environments (IDEs) and can be readily integrated with modern tools. As the level of the interface moves deeper into the legacy FORTRAN, more possibilities arise for improving the codebase quality and confidence in PROCESS output. It allows for better testing; the pytest testing framework has been implemented on the Continuous Integration (CI) system, which means that tests are much easier to write. This has already resulted in improved test coverage which helps isolate faults faster, ensures robust releases, and provides higher confidence in results. The Python conversion results in higher productivity for modellers; a familiar Python package layout makes for easier scripting and debugging. Standard Python logging and error handling improvements are in development. Development and testing of individual FORTRAN physics and engineering modules in isolation will become possible, facilitating comparison and scrutiny of models with other specialist groups. Data processing and analysis using the Python data structure will be much easier and consistent. Finally, the Python conversion allows for simple and reliable integration with other codes. PROCESS is easily installed as a Python package and an Application Programming Interface

(API) is now possible and in development. Developing and maintaining a consistent tested interface is crucial for utilising PROCESS in other codes (such as BLUEPRINT).

4. USHERING IN A NEW ERA OF SYSTEMS CODE (BLUEPRINT)

PROCESS, with its largely 0/1-D treatment of a wide variety of constraints, is an invaluable tool for exploring the future fusion reactor design space. Its output, however, is largely zero-dimensional and in terms of geometry only provides the reactor designer with a radial and vertical build. Whilst it constitutes a design point, it is not one which can be immediately used in higher fidelity studies which invariably require some form of 2-D or 3-D geometry. Furthermore, many of the constraints which PROCESS evaluates using a variety of simplified and surrogate models tend to be violated rather quickly when assessed at higher degrees of fidelity. Some constraints simply cannot be implemented in PROCESS due to lack of meaningful 2-D and 3-D geometry, and the need for generally more complicated and computationally expensive solvers. The design points generated in PROCESS are often transformed into more detailed reactor designs, with many higher fidelity models being used to generate more representative results for different aspects. When done manually, however, these procedures are expensive and can take many months to complete. With a view to delivering higher fidelity reactor designs, UKAEA has been developing a reactor design framework, BLUEPRINT, in which several models and codes (including PROCESS) are used in conjunction to automate fusion reactor design. A similar such framework is being developed in KIT: MIRA [31]. BLUEPRINT has a broad range of functionality, including toroidal field (TF) coil design, equilibria and poloidal field (PF) system design [32], 2-D geometry and 3-D CAD generation (with the goal of performing Monte Carlo neutronics simulations) [33], and fuel cycle modelling [34]. Presently in BLUEPRINT, several design activities are linked in series, starting from a PROCESS run and followed by a sequence of sub-system design optimisations, to progressively build a reactor design. Recently, BLUEPRINT has begun to be adapted for use in the UKAEA STEP project. This has led to a significant improvement of software quality (in preparation for collaborative development by a larger team). The documentation for BLUEPRINT was improved, computational speed optimisations were included, the test suite was enhanced, and several benchmarks and code comparisons were added. Novel developments have also been required for STEP, including new shape parameterisations, a simplified model to estimate heat fluxes due to charged particles on the first wall, PF coil position optimisation within regions, and new interfaces to different libraries (e.g. JETTO [35]) and more robust interfaces to existing ones (e.g. PROCESS). A command line interface was also developed, in preparation for distributed computing.

At present, the BLUEPRINT output is not internally consistent between levels of fidelity. PROCESS's calculation of the flat-top duration, for instance, is subsequently over-written by the PF system design optimisation step, which usually finds a lower value. Many more parameters and constraints evaluated in subsequent higher fidelity design activities are inconsistent with lower fidelity calculations. Thus, the resulting design does not meet the design requirements and in some places violates the specified design constraints. To address this, consistency constraints between the different levels of fidelity must be implemented, such that higher fidelity calculations override lower fidelity results and feed back into prior optimisation routines (most notably in PROCESS), iterating until convergence. This is a subject of future work and will clearly result in increased run-times. To strike a balance between fidelity and run-time, each set of consistency constraints will be implemented such that they are optionally enforced. This will provide the user with the capability to explore the design space broadly at low levels of fidelity, e.g., using only PROCESS, and progressively ramp up the degree of fidelity whilst narrowing the design space accordingly.

5. CONCLUSIONS AND OUTLOOK

The use of systems codes in power plant conceptual design will continue to offer useful input into the design workflow. Continuous improvements, outlined earlier in the paper, will enable codes like PROCESS and BLUEPRINT to offer relevant insight up to the engineering design phase of existing power plant projects as well as working on the first generation of commercial reactors. PROCESS and BLUEPRINT will continue to be used in the UKAEA STEP programme during the conceptual design phase. Both tools have been updated with spherical tokamak specific models that can better inform the design process. In the coming years (2021 onwards), under the auspices of a EUROfusion Theory Simulation Validation and Verification project, UKAEA and KIT plan to combine BLUEPRINT and MIRA into a single open-source reactor design framework, combining the

functionality of both. The aim of this project is to build this framework into a platform that users can perform rapid fusion power plant design analysis and produce detailed output, including 3-D CAD. Reactor design codes will remain useful tools going forward and incorporating new results allows for systems analysis to take place with increasing confidence in the output.

ACKNOWLEDGEMENTS

This work has been carried out within the framework of the EUROfusion Consortium and has received funding from the Euratom research and training programme 2014-2018 and 2019-2020 under grant agreement No 633053 and from the RCUK Energy Programme [grant number EP/T012250/1]. The views and opinions expressed herein do not necessarily reflect those of the European Commission.

REFERENCES

[1] M. Kovari, R. Kemp, H. Lux, P. Knight, J. Morris, and D. J. Ward, "" PROCESS " : A systems code for fusion power plants-Part 1: Physics," *Fusion Eng. Des.*, vol. 89, no. 12, pp. 3054–3069, Dec. 2014, doi: 10.1016/j.fusengdes.2014.09.018.

[2] M. Kovari *et al.*, "'PROCESS': A systems code for fusion power plants - Part 2: Engineering," *Fusion Eng. Des.*, vol. 104, pp. 9–20, Mar. 2016, doi: 10.1016/j.fusengdes.2016.01.007.

[3] J. Morris, R. Kemp, M. Kovari, J. Last, and P. Knight, "Implications of toroidal field coil stress limits on power plant design using PROCESS," *Fusion Eng. Des.*, vol. 98–99, pp. 1118–1121, 2015, doi: 10.1016/j.fusengdes.2015.06.100.

[4] H. Lux *et al.*, "Uncertainties in power plant design point evaluations," *Fusion Eng. Des.*, vol. 123, pp. 63–66, Nov. 2017, doi: 10.1016/j.fusengdes.2017.01.029.

[5] H. Lux, R. Kemp, D. J. Ward, and M. Sertoli, "Impurity radiation in DEMO systems modelling," *Fusion Eng. Des.*, vol. 101, pp. 42–51, Dec. 2015, doi: 10.1016/j.fusengdes.2015.10.002.

[6] G. Federici *et al.*, "Overview of the DEMO staged design approach in Europe," *Nucl. Fusion*, vol. 59, no. 6, p. 066013, Apr. 2019, doi: 10.1088/1741-4326/ab1178.

[7] J. Morris, V. Chan, J. Chen, S. Mao, and M. Y. Ye, "Validation and sensitivity of CFETR design using EU systems codes," *Fusion Eng. Des.*, vol. 146, pp. 574–577, Sep. 2019, doi: 10.1016/j.fusengdes.2019.01.026.

[8] S. I. Muldrew *et al.*, "'PROCESS': Systems studies of spherical tokamaks," *Fusion Eng. Des.*, vol. 154, 2020, doi: 10.1016/j.fusengdes.2020.111530.

[9] M. Coleman and S. McIntosh, "BLUEPRINT: A novel approach to fusion reactor design," *Fusion Eng. Des.*, vol. 139, pp. 26–38, Feb. 2019, doi: 10.1016/j.fusengdes.2018.12.036.

[10] M. Siccinio, G. Federici, R. Kembleton, H. Lux, F. Maviglia, and J. Morris, "Figure of merit for divertor protection in the preliminary design of the EU-DEMO reactor," *Nucl. Fusion*, vol. 59, no. 10, p. 106026, Oct. 2019, doi: 10.1088/1741-4326/ab3153.

[11] H. Zohm *et al.*, "A stepladder approach to a tokamak fusion power plant," *Nucl. Fusion*, vol. 57, no. 8, p. 086002, Aug. 2017, doi: 10.1088/1741-4326/aa739e.

[12] S. I. Muldrew, H. Lux, V. Menon, and R. Srinivasan, "Uncertainty analysis of an SST-2 fusion reactor design," *Fusion Eng. Des.*, vol. 146, pp. 353–356, Sep. 2019, doi: 10.1016/j.fusengdes.2018.12.066.

[13] F. Warmer, C. D. Beidler, A. Dinklage, and R. Wolf, "From W7-X to a HELIAS fusion power plant: Motivation and options for an intermediate-step burning-plasma stellarator," *Plasma Phys. Control. Fusion*, vol. 58, no. 7, p. 074006, Jun. 2016, doi: 10.1088/0741-3335/58/7/074006.

[14] F. Warmer *et al.*, "Implementation and verification of a HELIAS module for the systems code PROCESS," *Fusion Eng. Des.*, vol. 98–99, pp. 2227–2230, Oct. 2015, doi: 10.1016/j.fusengdes.2014.12.021.

[15] M. D. Morris, "Factorial sampling plans for preliminary computational experiments," *Technometrics*, vol. 33, no. 2, pp. 161–174, 1991, doi: 10.1080/00401706.1991.10484804.

[16] A. Saltelli *et al.*, *Global Sensitivity Analysis. The Primer*. Wiley, 2008.

[17] M. Kotschenreuther, P. M. Valanju, S. M. Mahajan, and J. C. Wiley, "On heat loading, novel divertors, and fusion reactors," *Phys. Plasmas*, vol. 14, no. 7, p. 072502, Jul. 2007, doi: 10.1063/1.2739422.

[18] P. M. Valanju, M. Kotschenreuther, S. M. Mahajan, and J. Canik, "Super-X divertors and high power density fusion devices," in *Physics of Plasmas*, May 2009, vol. 16, no. 5, p. 056110, doi: 10.1063/1.3110984.

[19] A. Pearce *et al.*, "Systems studies of double null divertor models," 2019.

[20] A. Kallenbach, M. Bernert, R. Dux, F. Reimold, and M. Wischmeier, "Analytical calculations for impurity seeded partially detached divertor conditions," *Plasma Phys. Control. Fusion*, vol. 58, no. 4, p. 045013, Apr. 2016, doi: 10.1088/0741-3335/58/4/045013.

[21] R. Heller, P. V. Gade, W. H. Fietz, T. Vogel, and K. P. Weiss, "Conceptual Design Improvement of a Toroidal Field Coil for EU DEMO Using High-Temperature Superconductors," *IEEE Trans. Appl. Supercond.*, vol. 26, no. 4, pp. 1–5, Jun. 2016, doi: 10.1109/TASC.2016.2520662.

[22] M. Ono and R. Kaita, "Recent progress on spherical torus research," *Phys. Plasmas*, vol. 22, no. 4, p. 040501, Apr. 2015, doi: 10.1063/1.4915073.

[23] F. Najmabadi *et al.*, "Spherical torus concept as power plants - The ARIES-ST study," *Fusion Eng. Des.*, vol. 65, no. 2, pp. 143–164, Feb. 2003, doi: 10.1016/S0920-3796(02)00302-2.

[24] H. R. Wilson *et al.*, "Integrated plasma physics modelling for the Culham steady state spherical tokamak fusion power plant," *Nucl. Fusion*, vol. 44, no. 8, pp. 917–929, Aug. 2004, doi: 10.1088/0029-5515/44/8/010.

[25] N. A. Uckan, "ITER physics design guidelines: 1989," 1990, [Online]. Available: http://www.iaea.org/inis/collection/NCLCollectionStore/_Public/21/068/21068960.pdf.

[26] O. Sauter, C. Angioni, and Y. R. Lin-Liu, "Neoclassical conductivity and bootstrap current formulas for general axisymmetric equilibria and arbitrary collisionality regime," *Phys. Plasmas*, vol. 6, no. 7, pp. 2834–2839, Jul. 1999, doi: 10.1063/1.873240.

[27] H. R. Wilson, "SCENE-Simulation of Self-Consistent Equilibria with Neoclassical Effects." 1994, Accessed: Mar. 30, 2021. [Online]. Available: http://inis.iaea.org/Search/search.aspx?orig_q=RN:26023312.

[28] J. E. Menard, "Compact steady-state tokamak performance dependence on magnet and core physics limits," in *Philosophical Transactions of the Royal Society A: Mathematical, Physical and Engineering Sciences*, Mar. 2019, vol. 377, no. 2141, doi: 10.1098/rsta.2017.0440.

[29] M. Wakatani *et al.*, "Plasma confinement and transport," *Nucl. Fusion*, vol. 39, no. 12, pp. 2175–2249, Dec. 1999, doi: 10.1088/0029-5515/39/12/302.

[30] M. Ono and R. Kaita, "Recent progress on spherical torus research," *Phys. Plasmas*, vol. 22, no. 4, p. 40501, Apr. 2015, doi: 10.1063/1.4915073.

[31] F. Franza, "Development and Validation of a Computational Tool for Fusion Reactors' System Analysis," 2019.

[32] M. Coleman and S. McIntosh, "The design and optimisation of tokamak poloidal field systems in the BLUEPRINT framework," *Fusion Eng. Des.*, vol. 154, p. 111544, May 2020, doi: 10.1016/j.fusengdes.2020.111544.

[33] M. Coleman, J. Shimwell, A. Davis, and S. McIntosh, "High-speed generation of neutronics-ready CAD models for DEMO design," *Fusion Eng. Des.*, vol. 160, p. 112043, Nov. 2020, doi: 10.1016/j.fusengdes.2020.112043.

[34] M. Coleman, Y. Hörstensmeyer, and F. Cismondi, "DEMO tritium fuel cycle: performance, parameter explorations, and design space constraints," *Fusion Eng. Des.*, vol. 141, pp. 79–90, Apr. 2019, doi: 10.1016/j.fusengdes.2019.01.150.

[35] G. Cenacchi and A. Taroni, "JETTO: A free-boundary plasma transport code (basic version)," 1988. Accessed: Mar. 19, 2021. [Online]. Available: http://inis.iaea.org/Search/search.aspx?orig_q=RN:19097143.